Journal of Earth Science, *Vol. 33*, *No. 1*, *p. 100−108*, *February 2022* *ISSN 1674-487X*
Printed in China
https://doi.org/10.1007/s12583-021-1490-3

A Preliminary Study on Silver Isotopic Composition in Polymetallic Ore Deposits in Eastern China

Ge Dong[1, 2], **Hai-Zhen Wei**[*1, 2], **Yuanfeng Zhu**[1], **Xi Liu**[1], **Qi Guo**[1], **Wei Pu**[1], **Yibo Lin**[1], **Junlin Wang**[1]

1. *State Key Laboratory for Mineral Deposits Research*, *Department of Earth Sciences and Engineering*, *Nanjing University*, *Nanjing* 210023, *China*

2. *CAS Center for Excellence in Comparative Planetology*, *China*, *Anhui* 230026, *China*

Ge Dong: https://orcid.org/0000-0001-6624-3409; Hai-Zhen Wei: https://orcid.org/0000-0002-6658-792X

ABSTRACT: A preliminary survey of silver isotopic composition in four polymetallic ores in eastern China shows a larger variation in δ^{109}Ag from -0.014‰ to +0.983‰, which is within the total ranges for the entire respective ore deposit types worldwide. The diversity of silver isotopic compositions in ore-deposits reported here and previous studies seemed to preclude simple isotopic links to particular sources, but reflected the silver isotope fractionation in transport- and deposit-related processes instead. The δ^{109}Ag values in supergene samples from the Qixiashan Pb-Zn-Ag polymetallic deposit are more positive, in consistent with the statistical δ^{109}Ag distribution from -0.4‰ to +2.2‰ in 36 pieces of supergene ore samples around the World, which reflects the diverse controls on silver isotope fractionation from the first-order thermodynamic effect, reduction-mediated reaction, remobilization of silver with surficial low-temperature weathering processes. The hypogene samples in Dazhuangzi orogenic Au-Ag ore deposit, have δ^{109}Ag values close to 0, which implies that equilibrium partitioning associated with metal sources at the high-temperature does not result in a resolvable difference in silver isotopic compositions. By contrast, the hypogene samples which are dominated by pyrite without visible silver minerals (i.e., skarn iron ore deposit in Edongnan) have shown the largest variation range of δ^{109}Ag, followed by that from the porphyry copper ore in Zijinshan. It could be concluded that the surface adsorption and/or lattice substitution are important factors to control Ag isotope fractionation in ore-forming processes, especially for skarn deposit with only pyrite. The perspective of silver isotope shows great potentials to understand the processes that lead to the concentrations of metals to economic levels and to constrain the physicochemical conditions during ore-mineralization in metallic ore-deposits.

KEY WORDS: silver isotopic composition, hypogene ore deposits, supergene ore deposits, metal transport, ore deposits.

0 INTRODUCTION

Silver is a precious metal and works as an indispensable material for modern industry and technology. Silver is a moderately volatile element that displays both siderophile and chalcophile behavior. As a common trace element in most terrestrial and extra-terrestrial rocks, it occurs at ~19 ng·g^{-1} in the pristine mantle and ~50 ng·g^{-1} in the upper continental crust level concentrations or higher (Taylor and McLennan, 1985). In nature, silver occurs as native silver, as alloys with gold, mercury, bismuth, copper, platinum, and as sulfides (e.g., argentite), sulfosalts (such as proustite and pyrargyrite) and silver halides (e.g., chlorargyrite), hosting in a variety of deposit-types, including epithermal, volcanogenic massive sulfides (VMS), sedimentary-exhalative (SEDEX), sediment-hosted Ag-Cu, carbonate replacement and skarns, porphyry Cu, mesothermal Ag-Pb-Zn, and Ag-Co-Ni-As veins (Kesler and Simon, 2015; Ayuso, 2010; Graybeal and Vikre, 2010). In recent years, the widespread discovery of these minerals has made gold and silver chalcogenides receive extensive attention (Zhu et al., 2021; Pal'Yanova et al., 2015; Savva et al., 2012; Plotinskaya et al., 2009).

Among 38 isotopes from ^{93}Ag to ^{130}Ag, silver has two stable isotopes of ^{107}Ag and ^{109}Ag with the following abundances of 51.839(51)% and 48.160(51)% (atom percentage) (Rosman and Taylor, 1998). The silver isotope composition is usually expressed as δ^{109}Ag as per mil deviation (‰) (Eq. 1) or ε^{109}Ag as ten thousand deviation (ε) (Eq. 2). It is reported as δ^{109}Ag (‰), relative to the NIST 978a, the certified stable silver isotope reference material in the silver isotope community here in this work.

$$\delta^{109}\mathrm{Ag} = \left(\frac{\left(^{109}\mathrm{Ag}/^{107}\mathrm{Ag}\right)_{\mathrm{sample}}}{\left(^{109}\mathrm{Ag}/^{107}\mathrm{Ag}\right)_{\mathrm{standard}}} - 1 \right) \times 1000 \qquad \text{(Eq. 1)}$$

*Corresponding author: haizhenwei@nju.edu.cn

Manuscript received March 26, 2021.
Manuscript accepted June 4, 2021.

Dong, G., Wei, H.-Z., Zhu, Y. F., et al., 2022. A Preliminary Study on Silver Isotopic Composition in Polymetallic Ore Deposits in Eastern China. *Journal of Earth Science*, 33(1): 100−108. https://doi.org/10.1007/s12583-021-1490-3. http://en.earth-science.net

$$\varepsilon^{109}\mathrm{Ag} = \left(\frac{(^{109}\mathrm{Ag}/^{107}\mathrm{Ag})_{\mathrm{sample}}}{(^{109}\mathrm{Ag}/^{107}\mathrm{Ag})_{\mathrm{standard}}} - 1 \right) \times 10\,000 \qquad \text{(Eq. 2)}$$

The analytical precision of ±0.05‰ in silver isotope measurement has been improved by one order of magnitude via using multi-collector inductively coupled plasma mass spectrometry (MC-ICP-MS) in recent decades, compared to that of ±1‰ to ±2‰ by the thermal ionization mass spectrometry (TIMS) (Woodland et al., 2005; Carlson and Hauri, 2001). For instance, the instrumental mass discrimination in the presence of matrix elements with dry plasma vs. wet plasma has been evaluated by Schönbächler et al. (2007). A three-stage ion-exchange procedure has been established to separate Ag from matrix elements such as Ti and Fe, resulting in an external reproducibility of ±0.05‰, which is suitable for terrestrial basalts and stony meteorites (Schönbächler et al., 2007). An efficient purification of Ag from environmental samples was obtained using a two-column ion-exchange procedure by Yang et al. (2010, 2009) and Luo et al. (2010), which yields an external reproducibility of ±0.04‰ in commercial Ag products and better than ±0.015‰ in environmental materials. The matrix effects originated from paragenetic minerals have been quantitatively evaluated, and the consequent modification of chemical chromatography ensured accurate analysis of silver isotopes in polymetallic ore-deposits (Guo et al., 2017).

The earlier studies of δ^{109}Ag in terrestrial rocks and meteorites demonstrated that silver isotope fractionation did not occur within the inner solar system during condensation of the solar nebular and chondrite parent body formation (Schönbächler et al., 2008). The silver isotopic composition (δ^{109}Ag) of +0.22 ±0.07 (2σ) was estimated for the bulk silicate Earth (BSE) relative to NIST 978a on the basis of mantle-derived samples (Schönbächler et al., 2010). With the understanding of the fractionation mechanism of silver isotopes in environmental processes, silver isotopes could provide a sensitive tool for fingerprinting the source of Ag in environmental cycling (Tolaymat et al., 2010). For instance, compared to the δ^{109}Ag values of -0.044‰, +0.025‰ and +0.061‰ in industrial sludge (SRM 2781), sediment (CRM PACS-2) and domestic sludge (SRM 2782), a larger positive value +0.284‰ observed in the fish liver (CRM DOLT-4) was attributed to silver isotope fractionation during biological uptakes (Luo et al., 2010). Besides, the adsorption of Ag ions makes heavy Ag isotope enriched in the solid phase (Lu et al., 2016). Compared to terrestrial rocks (Schönbächler et al., 2010, 2007; Woodland et al., 2005;), commercial products (Yang et al., 2009), environmental materials (Luo et al., 2010) and silver coins (Fujii and Albarede, 2018), much wider variations of δ^{109}Ag in metallic ore-deposits have been observed, such as in the Paleozoic orogenic Au deposits in Victorian Goldfields (Voisey et al., 2019), and in a gold mine in the Barberton Greenstone Belt (Argapadmi et al., 2018), as well as in a variety of mining districts on Earth (Arribas et al., 2020; Mathur et al., 2018). These findings indicated that there is no systematic δ^{109}Ag variation associated with mineralization age and temperature, deposit type and source rocks, recalling the understanding of mechanisms of silver isotope fractionation occurred in physicochemical processes related to transport and ore forming processes as well as the prevailing reduction reactions.

In China, the most common ore-bearing strata of silver deposits are Devonian, Mesoproterozoic and Carboniferous, and the output of silver deposits is controlled by marine volcanic, continental volcanic and intrusive rocks (Jiang et al., 2020). Silver deposits related to marine volcanic mainly distribute in the northwest and southwest of China, and that related to continental volcanic rocks distribute in eastern China, while deposits related to intrusive rocks are relatively widely distributed, mainly forming silver deposits of porphyry type and magmatic hydrothermal type (Jiang et al., 2020) (Fig. 1). The large-scale independent silver deposits dominated by silver are particularly rare in China, and there are many small and medium-sized symbioses and associated silver deposits. Because the metallogenic series and metallogenic lineages have a balanced temporal and spatial distribution, the types of silver deposits are gradually diversified with complex chemical composition and mineralization along with evolution. In addition, the metallogenic model is complicated, related to volcanism, hydrothermal process, sedimentation and metamorphism, and intermediate-acid magma intrusion. Therefore, there are still greater challenges in the study of the genesis and evolution mode of Au-Ag deposits.

In this study, four polymetallic ore deposits in eastern China are considered, including Zijinshan porphyry copper deposit, Dazhuangzi Orogenic Au-Ag ore deposit, Edongnan skarn iron deposit and Qixiashan polymetallic Pb-Zn-Ag ore deposit. We present the preliminary study of the isotopic composition of Ag in ore-deposits in China, in an attempt to explore the dominant factors that control the variation of δ^{109}Ag in ore-deposits, including hypogene and supergene processes, deposit type, mineralogical and chemical effects.

1 GEOLOGICAL SETTING

Four typical polymetallic ore deposits were selected, with reference to the distribution of silver deposits in China (Fig. 1), including Dazhuangzi mine (LS epithermal deposit), Edongnan mine (skarn iron deposit), Zijinshan porphyry copper deposit, and Qiaxiashan polymetallic Pb-Zn-Ag ore deposit (IS epithermal deposit).

The Edongnan skarn iron deposit is located in the southern section of the middle and lower reaches of the Yangtze River metallogenic belt (Zhang, 1998). The tectonic movement in the Yanshan-Sichuan Period provided a channel for magma to invade upward, causing various scales of mineralization (Zhang, 1998). There are a large number of magmatic rocks in the area. The rock masses are mainly Jurassic−Cretaceous intermediate and acidic intrusions, where a large amount of skarn-type iron occurs (Xie et al., 2006). Copper ore and most of the iron ore minerals in skarn iron ore are magnetite. The deposit is of high grade, easy to select, and has many economically useful components (Xie et al., 2006).

The Dazhuangzi gold mine in Jiaodong Peninsula is located in the southeastern margin of the North China Craton, it is on the east side of the near Yimu fault zone and the north side of the Jiaolai Basin (Liu et al., 2011). The host surrounding rocks are mainly Early Cambrian metamorphic rocks (mainly in the Jingshan Group), and there are almost no Mesozoic gra-

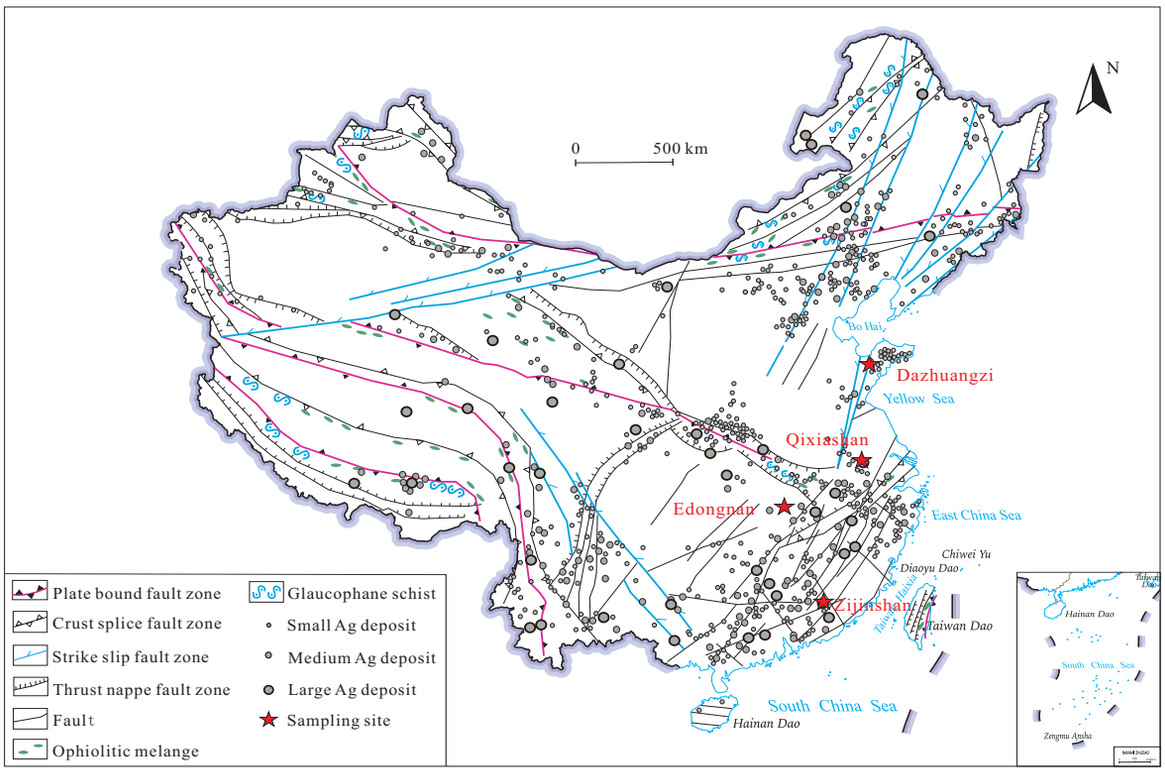

Figure 1. Distribution of small, medium and large silver deposits in China (modified after Jiang et al., 2020) and locations of sampling sites in eastern China in this study.

nitic intrusive rocks in the mining area (Liu et al., 2011; Zhu et al., 1999). The main mineralization temperature in the Dazhuangzi mining area is around 250 ºC (Liu et al., 2011). The recent investigation proposed that phase separation occurred during the mineralization process, which may lead to the enrichment of useful mineral components and the formation of deposits.

Zijinshan porphyry copper deposit is the largest hydrothermal copper-gold deposit with high sulfide and low temperature in mainland China (Zhang, 2013). It is an Ag-Au deposit related to high-potassium calcium-alkaline dacite-rhyolite on the continental margin (Jiang et al., 2013). Its main mineralization feature is the appearance of pyrite, diorite and breccia (Zhang, 2013). Copper (molybdenum) deposits and LS epithermal type silver-gold deposits are the main types of deposits (Huang, 2008). The Yueyang large-scale silver-gold-copper deposit is a typical LS epithermal deposit developed within the porphyritic dacites and crypto-explosive breccias in the Zijinshan mine field in Fujian Province (Jiang et al., 2015). The silver-gold-copper ore bodies mainly occur in the Zijinshan-like layered and lenticular granites, and are controlled by a series of low-angle NW-shovel-shaped faults (Jiang et al., 2017; Zhong et al., 2017).

Qixiashan Pb-Zn-Ag polymetallic deposit in Jiangsu is the largest lead-zinc polymetallic deposit in the Ningzhen ore concentration zone in the iron-copper, lead-zinc, and gold polymetallic metallogenic belt. It is also the largest lead-zinc-silver polymetallic deposit in East China (Zhang et al., 2017; Gui and Jing, 2011; Xu and Zeng, 2006). Pyrite, sphalerite and galena that show typical hydrothermal structures and textures are the main sulfide minerals that can help us explore the mineralization process (Sun et al., 2018). The locations of sampling sites are shown in Fig. 1.

2 MATERIALS AND METHODS

2.1 Materials

Milli-Q water (resistivity = 18.2 MΩ·cm) was used throughout the experiments, and concentrated HCl and HNO_3 were prepared through the sub-boiling distillation of commercial acids (AR) twice, using Savillex distillers. The NIST SRM 978a is the only universally available Ag isotope standard. It has a certified absolute isotopic ratio, $^{109}Ag/^{107}Ag = 0.929\,04 \pm 0.000\,22$ (Powell et al., 1982). A stock solution containing 1 000 μg·g^{-1} of Ag was prepared by quantitative dissolution of NIST SRM 978a (in $AgNO_3$ form) in 2% (*v*/*v*) HNO_3 solution and was diluted to 100 ng·g^{-1} (i.e., 100 ppb) for silver isotope analysis.

2.2 Dissolution of Ore-Deposit Samples

The fresh samples are crushed into powder of 200 meshes, and about 0.01−0.07 g of ore deposit sample powder was weighted and digested in a mixture of 2 mL of 12 mol·L^{-1} HF and 1 mL of 15 mol·L^{-1} HNO_3 in a closed Savillex Teflon beaker on a hot plate at 110 °C for two days. After the sample has been dried, 6 M HNO_3 was added, and the sample was left for a day to dry again on a hot plate. Subsequently, 6 M HCl was added and heated overnight to complete the dissolution. After further drying, the residues were dissolved in 30 mL of 0.5 M HCl. With the procedure, all geological standards and ore deposit samples were totally dissolved, and a small amount of black insoluble residues in orogenic-type ore deposit samples

were identified to be organic matter not containing any silver. The solutions were centrifuged for a few minutes before loading the supernatant into the column for matrix separation.

2.3 Ion-Exchange Chromatography

A two-column ion-exchange procedure was modified by our group recently to separate and purify trace Ag from minerals (Guo et al., 2017), on the basis of previous contributions by Schönbächler et al. (2007) and Luo et al. (2010). In the first step, 1.25 mL of anion exchange resin (AG1-X8, 100−200 mesh) was loaded in a 10 mL polypropylene Muromac® column with an internal diameter of 5 mm, that was cleaned and preconditioned with 30 mL of 2 M HCl and 15 mL 0.5 M HCl in sequence. One sample aliquot of ca. 1 μg of Ag was loaded into the pretreated columns. The matrix elements were eluted with 30 mL of 0.1 M HCl and 15 mL of 0.01 M HCl. Afterwards, another 1.8 mL of cation exchange resin (AG50W-X8, 200−400 mesh) was loaded into a 10 mL of polypropylene Muromac® column, which was cleaned and preconditioned by 60 mL of 6 M HNO_3 twice. In the second step, the first 1.25 mL of anion resin column connects with the second 1.8 mL of cation resin column in series. And then the columns were rinsed with 10 mL of 0.5 M HNO_3 to remove cation matrices such as Pb, Zn, Cu, Cd, Fe etc., and the Ag was eluted from the resins with 15 mL of 3.0 HNO_3. The details have been listed in Table 1, and the mean Ag recovery from the ion exchange protocols for silver separation and purification was greater than 96.5% (2SD, $n \geqslant 5$) in this study. Considering the high contents of impurities matrices that might induce obvious isobaric interferences on the silver isotope analysis, two runs of column chemistry were used. After the second run of column separation, the matrix ions that induce possible isobaric interferences on silver isotope (e.g., $^{65}Cu^{40}Ar^{+}$, $^{66}Zn^{40}Ar^{+}$, $^{67}Zn^{40}Ar^{+}$, $^{68}Zn^{40}Ar^{+}$, and Pb^{2+}) could be effectively removed, with the molar ratios of Fe/Ag, Zn/Ag, Cu/Ag, Cd/Ag, Sn/Ag and Pd/Ag less than 0.037, 2.291, 0.017, 0.137, 0.064 and 0.003 mol/mol respectively. Our previous doping experiment has shown that the proper selection of alternative Pd isotope pairs is one of effective ways to eliminate spectral matrix effects so as to ensure accurate analysis under the largest possible ranges for metal impurities (i.e., Cu/Ag ⩽ 50 : 1, Fe/Ag ⩽ 600 : 1, Pb/Ag ⩽ 10 : 1, and Zn/Ag ⩽ 1 : 1, respectively (Guo et al., 2017). The combination of an appropriate Pd isotope pair and the modified ion-exchange procedure ensures accurate analysis of silver isotope in polymetallic ore-deposits in this study.

2.4 Silver Isotope Analysis

A Neptune Plus MC ICP-MS (Thermo Fisher Finnigan) with an ESI PFA 50 μL/min nebulizer in a quartz cyclonic spray chamber was used for the measurement of silver isotopic composition. The ions $^{107}Ag^{+}$ and $^{109}Ag^{+}$ were detected using Faraday Cups C and H2, and $^{104}Pd^{+}$, $^{105}Pd^{+}$, $^{106}Pd^{+}$, $^{108}Pd^{+}$ were detected using Faraday cups L3, L2, L1 and H1, with 10^{11} Ω amplifiers in all cases. The mass bias was corrected by standard-sample-bracketing procedure (SSB) following the procedure proposed by Luo et al., (2010). The silver content in both the sample solution and the NIST 978a standard solution was kept at around 100 ng·mL^{-1}, resulting in ~1.2 V of signal on $^{107}Ag^{+}$ with the conventional H-skimmer cone. To avoid memory effects, we washed the inlet system with 3% HNO_3 and Milli-Q water in sequence for ~10 minutes between measurements to reduce the signals to ~3 mV (An and Huang, 2014). All reproducibility described in this work is quoted from repeated measurements of the samples ($n \geqslant 5$, 2SD, 95% confidence limits). The average internal analytical precision (n = 40, 4 blocks × 10 cycles) of the measured $^{109}Ag/^{107}Ag$ ratios of 100 ng·mL^{-1} NIST 978a is 0.02‰ and the long-term external reproducibility is 0.012‰ ($n \geqslant 10$) (Fig. 2). The typical operating conditions are summarized in our previous contribution (Guo et al., 2017).

2.5 Elemental Composition Analysis

The element concentrations of the ore-deposit samples were analyzed on an ICP-MS (Finnigan Element II) at the State Key Laboratory for Mineral Deposits Research, Nanjing University. The signal drift during ICP-MS measurement was corrected by adding Rh solutions of known concentration with an analytical reproducibility better than ± 5%.

3 RESULTS

The silver isotopic compositions and concentrations of Ag, Pb, Zn, Cu and Fe for the Au-Ag deposits in eastern China

Table 1 Silver separation and purification procedure by the two-step ion exchange column

Step	Procedure	Reagents	Dosage (mL)
First column-1.25 mL of anion exchange resin (AG1-X8, 100−200 mesh)			
1	Loading column	AG1-X8	1.25
2	Cleaning	2 M HCl	30
3	Preconditioning	0.5 M HCl	15
4	Loading sample	0.5 M HCl	30
5	Rinsing matrix	0.5 M HCl	50
6	Rinsing matrix	0.1 M HCl	30
7	Rinsing matrix	0.01 M HCl	15
8	Eluting cations	0.5 M HNO3	30
9	Eluting Ag	3.0 M HNO3	15
Second column-1.8 mL of cation exchange resin (AG50W-X8, 200−400 mesh)			
1	Loading column	AG50W-X8	1.8
2	Cleaning	6.0 M HNO3	30
3	Preconditioning	6.0 M HNO3	30
4	Eluting cations	0.5 M HNO3	30
5	Eluting Ag	3.0 M HNO3	15

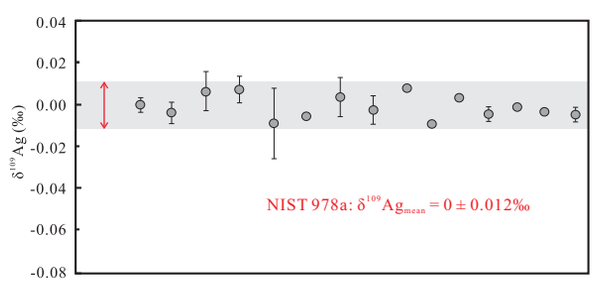

Figure 2. Long-term reproducibility of silver isotope analysis in the silver isotope standard reference material NIST 978a.

are shown in Table 2. The silver content in ore-deposit samples ranges from 0.17 to 109 $\mu g \cdot g^{-1}$, while the contents of Pb, Zn and Cu are from 20 to 11 440 $\mu g \cdot g^{-1}$, from 70 to 3 370 $\mu g \cdot g^{-1}$ and 60 to 32 800 $\mu g \cdot g^{-1}$. Iron contents are 4 or 5 orders of magnitude higher than Ag, ranging from 19 000 to 510 000 $\mu g \cdot g^{-1}$. The silver isotopic composition $\delta^{109}Ag$ ranges from -0.014‰ to +0.935‰, in which the $\delta^{109}Ag$ values in samples from the Dazhuangzi mine (LS epithermal) show more negative than the bulk silicate Earth (BSE), in a narrow range from -0.043‰ to +0.138‰, and these for other three mines (i.e., from -0.039‰ to +0.934‰ in skarn iron deposit in Edongnan, from +0.369‰ to +1.017‰ in porphyry copper deposit in Zijinshan, and from +0.449‰ to +0.930‰ in IS epithermal deposit in Qixiashan) are more positive to BSE. There is no correlation between $\delta^{109}Ag$ and the chemical compositions in these ore samples.

4 DISCUSSION

4.1 Distribution of $\delta^{109}Ag$ within Different Deposit Types

Four deposit types are included in this study to compare with the distribution of $\delta^{109}Ag$ in ore deposits over 30 countries worldwide, and then to discuss the effects of the genetic processes on the $\delta^{109}Ag$ values (Fig. 3). After Schönbächler et al. (2007) and Woodland et al. (2005) measured the $\delta^{109}Ag$ values of Hawaiian basalt (KOO 49-1) to be +0.935‰ ± 0.068‰ (2σ) and 1.046‰ ± 0.025‰ (2σ), a more negative $\delta^{109}Ag$ value of -0.577‰ ± 0.012‰ (2σ) for the same Hawaiian basalt (KOO 49-1) was reported by Theis et al. (2013) later. The controversial results reflect the difficulty in accurate analysis of silver isotopes in rocks and sediments because of the low abundance of silver in continental crust and mantle materials.

The wide variation $\delta^{109}Ag$ from -0.014 to +0.935‰ in ore deposits from this study is comparable to the range from -1 to +2‰ from previous contributions (Arribas et al., 2020; Voisey et al., 2019; Argapadmi et al., 2018; Mathur et al., 2018). Importantly, from the perspective of this study, the large variation of $\delta^{109}Ag$ values in ore-deposits was used to make inferences about the processes that lead to the concentrations of metals to economic levels and to constrain the physicochemical conditions during ore-mineralization. The variations of $\delta^{109}Ag$ in four individual deposit types from this study are within the total ranges for the entire respective ore deposit types and no systematic $\delta^{109}Ag$ to characterize a specific type of deposit (Fig. 3). The results argue against the inheritance of $\delta^{109}Ag$ signatures from sources rocks, and an alternative explanation for the silver isotope variation might be mass-dependent isotope fractionation in transport and co-precipitation of Ag-bearing minerals during hydrothermal ore formation. So far, the lack of a sufficient $\delta^{109}Ag$ dataset of terrestrial rocks makes it hard to define the silver isotope characteristics in the terrestrial reservoirs (e.g., the upper continental crust and the mantle). Therefore, it remains a great challenge to use silver isotope as a source tracer for Au-Ag ore deposits.

4.2 Distribution of $\delta^{109}Ag$ with Mineral Assemblage and Metallogenic Environment

When grouped as metallogenic environments, the $\delta^{109}Ag$ values in supergene samples from the Qixiashan Pb-Zn-Ag polymetallic deposit are more positive (Fig. 4), in consistent with the statistical $\delta^{109}Ag$ distribution from -0.4 to +2.2‰ in 36 pieces of supergene samples by Arribas et al. (2020). It might be attributed to the nuclear volume effect associated with the reduction-mediated reaction, surface adsorption and precipitation reactions associated with surficial low-temperature weathering processes, as suggested by Chugaev and Chernyshev

Table 2 Silver isotopic and elemental compositions in ore-deposit samples in eastern China

Sample No.	Mining district	Deposit type	Minerals	$\delta^{109}Ag$ (‰, 2σ, $n \geq 4$)	Ag (μg/g)	Pb (mg/g)	Zn (mg/g)	Cu (mg/g)	Fe (mg/g)
ZK23-12-H30	Dazhuangzi	LS epithermal	Galena, sphalerite, argentite	-0.014 (0.029)	109.32	1.31	2.63	0.22	22.17
ZK23-12-H32	Dazhuangzi	LS epithermal	Galena, sphalerite, argentite	+0.067 (0.071)	27.59	11.44	3.37	0.06	19.07
160u-09	Edongnan	Skarn	Bornite, chalcopyrite	+0.689 (0.010)	3.97	0.07	0.12	591	139
160u-33	Edongnan	Skarn	Pyrite	+0.552 (0.027)	3.84	0.49	0.29	328	326
16RJW-45	Edongnan	Skarn	Pyrite	+0.472 (0.086)	3.33	0.05	0.20	2.01	480
16LJS-01	Edongnan	Skarn	Pyrite	+0.924 (0.010)	3.37	0.03	0.06	1.46	486
16LJS-05	Edongnan	Skarn	Pyrite	+0.591 (0.024)	3.85	0.05	0.07	0.82	479
16FJS-13	Edongnan	Skarn	Pyrite	+0.007 (0.046)	2.07	0.03	0.18	1.09	504
16FJS-27	Edongnan	Skarn	Pyrite	+0.359 (0.049)	2.10	0.05	0.08	2.00	489
312-2	Zijinshan	Porphyry copper	Pyrite, natural silver, argentite	+0.935 (0.027)	0.19	0.02	*	0.15	371
312-4	Zijinshan	Porphyry copper	Pyrite, natural silver, argentite	+0.983 (0.034)	0.47	0.02	0.19	0.11	399
312-5	Zijinshan	Porphyry copper	Pyrite, natural silver, argentite	+0.846 (0.061)	0.17	0.02	0.04	0.08	480
312-15	Zijinshan	Porphyry copper	Pyrite, natural silver, argentite	+0.548 (0.180)	0.23	0.02	0.08	0.14	486
312-20	Zijinshan	Porphyry copper	Pyrite, natural silver, argentite	+0.631 (0.068)	0.28	0.07	0.07	0.16	479
4801-6	Qixiashan	IS epithermal	Pyrite, natural silver, argentite	+0.619 (0.106)	0.42	0.14	2.88	0.15	396
4201-26	Qixiashan	IS epithermal	Pyrite, natural silver, argentite	+0.548 (0.054)	0.45	0.24	1.75	0.11	440
4201-16	Qixiashan	IS epithermal	Pyrite, natural silver, argentite	+0.503 (0.054)	0.41	0.26	2.66	0.08	429
4602-7	Qixiashan	IS epithermal	Pyrite, natural silver, argentite	+0.716 (0.214)	0.53	0.87	0.35	0.14	452
4602-17	Qixiashan	IS epithermal	Pyrite, natural silver, argentite	+0.745 (0.180)	0.42	0.15	0.65	0.16	510

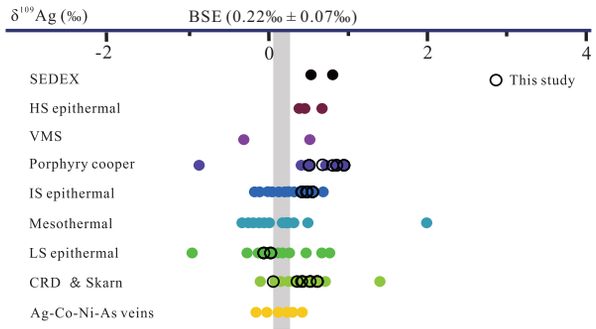

Figure 3. The distribution of silver isotopes in ore deposits with different types in this study and the previous contributions (Arribas et al., 2020; Voisey et al., 2019; Argapadmi et al., 2018; Mathur et al., 2018).

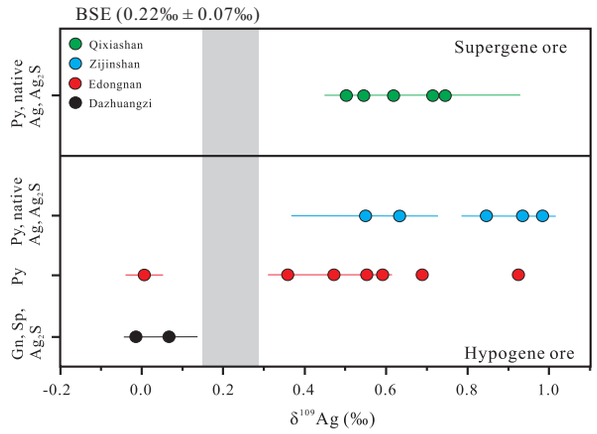

Figure 4. Silver isotopic compositions grouped by minerals assemblage and metallogenic environments.

(2012), Mathur et al. (2018), Fujii and Albarede (2018), Voisey et al. (2019) and Arribas et al. (2020). By contrast, the hypogene samples in Dazhuangzi with the minerals assemblage of galena, sphalerite, argentite have δ^{109}Ag values close to 0, which might reflect equilibrium partitioning associated with metal sources at the high-temperature that does not result in a resolvable difference in silver isotopic compositions. It is worth noting that the hypogene samples which are dominated by pyrite without visible silver minerals (i.e., skarn iron ore deposit in Edongnan) have shown the largest variation range of δ^{109}Ag, followed by the minerals assemblage of pyrite, native Ag and argentite in the porphyry copper ore in Zijinshan. In the skarn iron ore deposit in Edongnan, the fluid did not deposit native silver or argentite, and we concluded that it was undersaturated in respect to these minerals. Instead of precipitating directly from the fluid, silver was concentrated by adsorption onto the surface growing pyrite crystals. Adsorption of gold and silver onto pyrite has been proposed previously as a mechanism to explain the occurrence of "invisible gold" in other epithermal deposits (e. g., Pals et al., 2003; Widler and Seward, 2002). In addition, the corporation of Au and Ag in the pyrite structure is favored by trace quantities of As with the Au + As substitution for Fe in pyrite structure (Huston et al., 1995), and by the presence of Te, which substitutes for the smaller S ion, thereby expanding the lattice and providing space for the large Au and Ag ions (Chouinard et al., 2005). Therefore, the potential silver isotope fractionation during incorporation of silver into pyrite crystal might be complicated, which involves both surface adsorption and lattice substitution. The kinetic isotope fractionations that occurred in the interface reaction have been extensively studied, such as boron adsorption onto different minerals (e.g., Gaillardet, 2018). Therefore, it is critical to understand surface adsorption-induced silver isotope fractionation in the near future, in order to interpret the wide variation of δ^{109}Ag in hypogene ore deposits.

4.3 Factors that Control Silver Isotope Fractionation in Ore-Forming Processes

The interpretation of a large variation range in δ^{109}Ag in polymetallic ore deposits in worldwide might be complicated by a variety of physiochemical processes, including fluid phase separation (effervescence, boiling and condensation), multistage ore paragenesis, precipitation, reduction-mediated reaction. Besides, gold- and silver-bearing solids are commonly under-saturated in the condensed vapors and are able to concentrate through adsorption as negatively charged or neutral species onto the surfaces of growing pyrite crystals via lattice substitutions (King et al., 2014; Scher et al., 2013). The potential silver isotope fractionation could be classified as: (i) Metal transport-related process: the effects of vapor-liquid or liquid-liquid phase separation are commonly observed in shallow hydrothermal environments, such as porphyry and epithermal deposits (Heinrich et al., 1999). The solubility of Cu, Au and Ag in vapor phase is highly variable in magmatic-hydrothermal systems, depending on *P-T*, pH, salinity, and density, etc. (Migdisov and Williams-Jones, 2013). It could be concluded that, both the equilibrium and kinetic isotope effects during silver partitioning among phases need to be well concerned, in addition to the temperature-dependent equilibrium silver isotope fractionation in vapor-liquid and liquid-liquid phases. (ii) Ore-deposition process: In supergene ore-deposits (e. g., Qixiashan Pb-Zn-Ag polymetallic deposit in this study), the first-order thermodynamic effect on equilibrium silver isotope fractionation between minerals and fluids is determined to be significant as governed by Bigeleisen and Mayer approximation (Bigeleisen and Mayer, 1947). Besides, the sunlight-induced reduction reaction tends to be prevailing under shallow deposition conditions, where minerals such as chlorargyrite always suffer from decomposition under sunlight irradiation to produce native silver. Therefore, the nuclear volume effect (i. e., NVE) caused by *s*-electron occupational changes on isotope fractionation of silver must be taken into account (Voisey et al., 2019; Fujii and Albarede, 2018). Consequently, kinetic isotope effects from redox reaction and remobilization of silver with weathering make silver isotope signatures more complicated, as approved by more positive δ^{109}Ag distribution from the abundant dataset of IS epithermal samples from 69 deposits or districts from Arribas et al. (2020) and the Qixiashan Pb-Zn-Ag polymetallic deposit from this study (Fig. 3). In hypogene ore-deposits, the first-order thermodynamic effect on equilibrium silver isotope fractionation with minerals precipitation directly from saturated fluids might be limited (e. g., LS epithermal deposit in Dazhuangzi). However, the δ^{109}Ag signatures appeared to be difficult to explain, if the fluid was undersaturated in re-

spect to native silver and silver-bearing minerals or multiple stages of fluid were involved in the deposition processes. The typical examples from this study are the skarn iron ore deposit in Edongnan and the porphyry copper ore in Zijinshan with a much wider δ^{109}Ag variation range (Figs. 3, 4). It could be concluded that the surface adsorption and/or lattice substitution are important factors to control Ag isotope fractionation in ore-forming processes, especially for skarn deposit with only pyrite. There are diverse factors that could influence the kinetics of the surface adsorption of silver onto pyrite mineral, depending on the characteristics of the solution and solid surface, as the type and/or the number of active adsorption sites may vary with changing pH, chemical composition of solution as well as surface charge properties of solids. In combination with the multiple paths of silver incorporation into mineral lattice at either cation or anion position, larger silver isotope fractionations could be expected in the deposition processes of these type of ore-deposits.

5 CONCLUSION

A preliminary survey of silver isotopic composition in four polymetallic ores in eastern China shows a larger variation in δ^{109}Ag from -0.014‰ to +0.983‰, which is within the total ranges for the entire respective ore deposit types worldwide. The diversity of silver isotopic compositions in ore-deposits reported here and previous studies seemed to preclude simple isotopic links to particular sources (i.e., UCC-derived or mantle-derived) for the lack of sufficient δ^{109}Ag dataset of terrestrial rocks, but reflects the silver isotope fractionation in transport- and deposit-related processes instead. In metal transport process, both kinetic isotope effect during phase separation and temperature-dependent equilibrium isotope fractionation in vapor-liquid and liquid-liquid phases contributed to silver isotope variations. In supergene ores, the δ^{109}Ag values are more positive (e. g., the Qixiashan Pb-Zn-Ag polymetallic deposit), which could be attributed to the nuclear volume effect associated with reduction-mediated reaction, and remobilizations occurred with surficial low-temperature weathering processes. In hypogene ore-deposits, the δ^{109}Ag values vary either in a narrow range (e. g., Dazhuangzi orogenic Au-Ag ore deposit) or wider ranges (e.g., Edongnan skarn iron deposit, Zijinshan porphyry copper deposit), depending on the minerals assemblage of ore-deposits. On the basis of the current investigation, it is essential to understand silver isotope fractionation in physiochemical processes (e.g., phase separation (effervescence, boiling and condensation), multistage ore paragenesis, precipitation, redox, adsorption and remobilization etc.) and to define the silver isotope characteristics in terrestrial reservoirs in the near future.

ACKNOWLEDGMENTS

This research was supported by the National Natural Science Foundations of China (Nos. 41973005, 41673001), and China National Space Administration (CNSA) (No. D020205). The final publication is available at Springer via https://doi.org/10.1007/s12583-021-1490-3.

REFERENCES CITED

An, Y. J., Huang, F., 2014. A Review of Mg Isotope Analytical Methods by MC-ICP-MS. *Journal of Earth Science*, 25(5): 822−840. https://doi.org/10.1007/s12583-014-0477-8

Argapadmi, W., Toth, E. R., Fehr, M. A., et al., 2018. Silver Isotopes as a Source and Transport Tracer for Gold: A Reconnaissance Study at the Sheba and New Consort Gold Mines in the Barberton Greenstone Belt, Kaapvaal Craton, South Africa. *Economic Geology*, 113(7): 1553−1570. https://doi.org/10.5382/econgeo.2018.4602

Arribas, A., Mathur, R., Megaw, P., et al., 2020. The Isotopic Composition of Silver in Ore Minerals. *Geochemistry, Geophysics, Geosystems*, 21 (8): e2020gc009097. https://doi.org/10.1029/2020gc009097

Ayuso, R. A., 2010. Porphyry Copper Deposit Model: Chapter B in Mineral Deposit Models for Resource Assessment. In: John, D. A., ed., US Geological Survey, Reston. https://doi.org/10.3133/sir20105070b

Bigeleisen, J., Mayer, M. G., 1947. Calculation of Equilibrium Constants for Isotopic Exchange Reactions. *The Journal of Chemical Physics*, 15 (5): 261−267. https://doi.org/10.1063/1.1746492

Carlson, R. W., Hauri, E. H., 2001. Extending the ^{107}Pd-^{107}Ag Chronometer to Low Pd/Ag Meteorites with Multicollector Plasma-Ionization Mass Spectrometry. *Geochimica et Cosmochimica Acta*, 65(11): 1839−1848. https://doi.org/10.1016/s0016-7037(01)00559-2

Chouinard, A., Paquette, J., Williams-Jones, A. E., 2005. Crystallographic Controls on Trace-Element Incorporation in Auriferous Pyrite from the Pascua Epithermal High-Sulfidation Deposit, Chile Argentina. *The Canadian Mineralogist*, 43(3): 951−963. https://doi. org/10.2113/gscanmin.43.3.951

Chugaev, A. V., Chernyshev, I. V., 2012. High-Noble Measurement of 107Ag/109Ag in Native Silver and Gold by Multicollector Inductively Coupled Plasma Mass Spectrometry (MC-ICP-MS). Geochemistry International, 50(11): 899−910. https://doi. org/10.1134/S0016702912110055

Fujii, T., Albarede, F., 2018. ^{109}Ag-^{107}Ag Fractionation in Fluids with Applications to Ore Deposits, Archeometry, and Cosmochemistry. *Geochimica et Cosmochimica Acta*, 234: 37−49. https://doi. org/10.1016/j.gca.2018.05.013

Gaillardet, J., 2018. Boron in the Weathering Environment. In: Lemarchand, D., Marschall, H., Foster, G., eds., Boron Isotopes, Advances in Isotope Geochemistry. Springer, Cham. https://doi. org/10.1007/978-3-319-64666-4_7

Graybeal, F. T., Vikre, P. G., 2010. A Review of Silver-Rich Mineral Deposits and Their Metallogeny. In: The Challenge of Finding New Mineral Resources: Global Metallogeny, Innovative Exploration, and New Discoveries. https://doi.org/10.5382/sp.15.1.07

Gui, C. J., Jing, S., 2011. Ore-Forming Properties and Prospect of Pb-Zn Polymetallic Ore Deposit in Qixia Mountain of Nanjing. *Journal of Geology*, 35(4): 395−400. https://doi.org/10.3969/j.issn.1674-3636 (in Chinese with English Abstract)

Guo, Q., Wei, H. Z., Jiang, S. Y., et al., 2017. Matrix Effects Originating from Coexisting Minerals and Accurate Determination of Stable Silver Isotopes in Silver Deposits. *Analytical Chemistry*, 89(24): 13634−13641. https://doi.org/10.1021/acs.analchem.7b04212

Heinrich, C. A., Günther, D., Audétat, A., et al., 1999. Metal Fractionation between Magmatic Brine and Vapor, Determined by Microanalysis of Fluid Inclusions. *Geology*, 27(8): 755−758. https://doi. org/10.1130/0091-7613(1999)027<0755:mfbmba>2.3.co;2

Huang, R. S., 2008. Igneous Series and Epithermal Porphyry Cu-Au-Ag Mineralization System in the Zijinshan Ore Field, Fujian Province.

Journal of Geomechanics, 14: 74−86 (in Chinese with English Abstract)

Huston, D. L., Sie, S. H., Suter, G. F., et al., 1995. Sulfide Deposits: Part I. Proton Microprobe Analyses of Pyrite, and Part II. Selenium Levels in Pyrite: Comparison with $\delta^{34}S$ Values and Implications for the Source of Sulfur in Volcanogenic Hydrothermal Systems. *Economic Geology*, 90: 1167−1196. https://doi.org/10.2113/gsecongeo.90.5.1167

Jiang, B., Zhang, T., Wang, D. H., et al., 2020. Factors Controlling Ore Formation, Regularity and Some Prospecting Strategies for Silver Deposits in China. *Acta Geologica Sinica*, 94: 113−126 (in Chinese with English Abstract)

Jiang, S. H., Bagas, L., Liang, Q. L., 2015. New Insights into the Petrogenesis of Volcanic Rocks in the Shanghang Basin in the Fujian Province, China. *Journal of Asian Earth Sciences*, 105: 48−67. https://doi.org/10.1016/j.jseaes.2015.03.027

Jiang, S. H., Bagas, L., Liang, Q. L., 2017. Pyrite Re-Os Isotope Systematics at the Zijinshan Deposit of SW Fujian, China: Constraints on the Timing and Source of Cu-Au Mineralization. *Ore Geology Reviews*, 80: 612−622. https://doi.org/10.1016/j.oregeorev.2016.07.024

Jiang, S. H., Liang, Q. L., Bagas, L., et al., 2013. Geodynamic Setting of the Zijinshan Porphyry-Epithermal Cu-Au-Mo-Ag Ore System, SW Fujian Province, China: Constrains from the Geochronology and Geochemistry of the Igneous Rocks. *Ore Geology Reviews*, 53: 287−305. https://doi.org/10.1016/j.oregeorev.2013.02.001

Kesler, S. E., Simon, A. C., 2015. Mineral Resources, Economics and the Environment. In: Simon, A. C., ed.. Cambridge University Press, Cambridge. https://doi.org/10.1017/cbo9781139871426

King, J., Williams-Jones, A. E., van Hinsberg, V., et al., 2014. High-Sulfidation Epithermal Pyrite-Hosted Au (Ag-Cu) Ore Formation by Condensed Magmatic Vapors on Sangihe Island, Indonesia. *Economic Geology*, 109(6): 1705−1733. https://doi. org/10.2113/econgeo.109.6.1705

Liu, X., Fan, H. R., Hu, F. F., et al., 2011. Ore-Forming Fluid and Stable Isotope Studies of Dazhuangzi Gold Deposit in Jiaodong Peninsula. *Mineral Deposits*, 30(4): 675−689. https://doi. org/10.16111/j. 0258-7106.2011.04.007 (in Chinese with English Abstract)

Lu, D. W., Liu, Q., Zhang, T. Y., et al., 2016. Stable Silver Isotope Fractionation in the Natural Transformation Process of Silver Nanoparticles. *Nature Nanotechnology*, 11(8): 682−686. https://doi.org/10.1038/nnano.2016.93

Luo, Y., Dabek-Zlotorzynska, E., Celo, V., et al., 2010. Accurate and Precise Determination of Silver Isotope Fractionation in Environmental Samples by Multicollector-ICPMS. *Analytical Chemistry*, 82(9): 3922−3928. https://doi.org/10.1021/ac100532r

Mathur, R., Arribas, A., Megaw, P., et al., 2018. Fractionation of Silver Isotopes in Native Silver Explained by Redox Reactions. *Geochimica et Cosmochimica Acta*, 224: 313−326. https://doi. org/10.1016/j.gca.2018.01.011

Migdisov, A. A., Williams-Jones, A. E., 2013. A Predictive Model for Metal Transport of Silver Chloride by Aqueous Vapor in Ore-Forming Magmatic-Hydrothermal Systems. *Geochimica et Cosmochimica Acta*, 104: 123−135. https://doi.org/10.1016/j.gca.2012.11.020

Pal'Yanova, G., Mikhlin, Y., Kokh, K., et al., 2015. Experimental Constraints on Gold and Silver Solubility in Iron Sulfides. *Journal of Alloys and Compounds*, 649: 67−75. https://doi. org/10.1016/j.jallcom.2015.07.131

Pals, D. W., Spry, P. G., Chryssoulis, S. L., 2003. Invisible Gold and Tellurium in Arsenic-Rich Pyrite from the Emperor Gold Deposit, Fiji: Implications for Gold Distribution and Deposition. *Economic Geology*, 98(3): 479−493. https://doi.org/10.2113/gsecongeo.98.3.479

Plotinskaya, O. Y., Groznova, E. O., Kovalenker, V. A., et al., 2009. Mineralogy and Formation Conditions of Ores in the Bereznyakovskoe Ore Field, the Southern Urals, Russia. *Geology of Ore Deposits*, 51(5): 371−397. https://doi.org/10.1134/S1075701509050031

Powell, L. J., Murphy, T. J., Gramlich, J. W., 1982. The Absolute Isotopic Abundance and Atomic Weight of a Reference Sample of Silver. *Journal of Research of the National Bureau of Standards*, 87(1): 9. https://doi.org/10.6028/jres.087.002

Rosman, K. J. R., Taylor, P. D. P., 1998. Isotopic Compositions of the Elements 1997 (Technical Report). *Pure and Applied Chemistry*, 70(1): 217−235. https://doi.org/10.1351/pac199870010217

Savva, N. E., Pal'yanova, G. A., Byankin, M. A., 2012. The Problem of Genesis of Gold and Silver Sulfides and Selenides in the Kupol Deposit (Chukotka, Russia). *Russian Geology and Geophysics*, 53(5): 457−466. https://doi.org/10.1016/j.rgg.2012.03.006

Scher, S., Williams-Jones, A. E., Williams-Jones, G., 2013. Fumarolic Activity, Acid-Sulfate Alteration, and High Sulfidation Epithermal Precious Metal Mineralization in the Crater of Kawah Ijen Volcano, Java, Indonesia. *Economic Geology*, 108(5): 1099−1118. https://doi.org/10.2113/econgeo.108.5.1099

Schönbächler, M., Carlson, R. W., Horan, M. F., et al., 2007. High Precision Ag Isotope Measurements in Geologic Materials by Multiple-Collector ICPMS: An Evaluation of Dry Versus Wet Plasma. *International Journal of Mass Spectrometry*, 261(2/3): 183−191. https://doi. org/10.1016/j.ijms.2006.09.016

Schönbächler, M., Carlson, R. W., Horan, M. F., et al., 2008. Silver Isotope Variations in Chondrites: Volatile Depletion and the Initial ^{107}Pd Abundance of the Solar System. *Geochimica et Cosmochimica Acta*, 72 (21): 5330−5341. https://doi.org/10.1016/j.gca.2008.07.032

Schönbächler, M., Carlson, R. W., Horan, M. F., et al., 2010. Heterogeneous Accretion and the Moderately Volatile Element Budget of Earth. *Science*, 328(5980): 884−887. https://doi.org/10.1126/science.1186239

Sun, X. J., Ni, P., Yang, Y. L., et al., 2018. Formation of the Qixiashan Pb-Zn Deposit in Middle-Lower Yangtze River Valley, Eastern China: Insights from Fluid Inclusions and in Situ LA-ICP-MS Sulfur Isotope Data. *Journal of Geochemical Exploration*, 192: 45−59. https://doi.org/10.1016/j.gexplo.2018.03.011

Taylor, S. R., McLennan, S. M, 1985. The Continental Crust: Its Composition and Evolution. Blackwell, London. 57−72

Theis, K. J., Schönbächler, M., Benedix, G. K., et al., 2013. Palladium-Silver Chronology of IAB Iron Meteorites. *Earth and Planetary Science Letters*, 361: 402−411. https://doi. org/10.1016/j.epsl.2012.11.004

Tolaymat, T. M., El Badawy, A. M., Genaidy, A., et al., 2010. An Evidence-Based Environmental Perspective of Manufactured Silver Nanoparticle in Syntheses and Applications: A Systematic Review and Critical Appraisal of Peer-Reviewed Scientific Papers. *Science of the Total Environment*, 408(5): 999−1006. https://doi. org/10.1016/j.scitotenv.2009.11.003

Voisey, C. R., Maas, R., Tomkins, A. G., et al., 2019. Extreme Silver Isotope Variation in Orogenic Gold Systems Implies Multistaged Metal Remobilization during Ore Genesis. *Economic Geology*, 114(2): 233−242. https://doi.org/10.5382/econgeo.2019.4629

Widler, A. M., Seward, T. M., 2002. The Adsorption of Gold(I) Hydrosulphide Complexes by Iron Sulphide Surfaces. *Geochimica et Cosmochimica Acta*, 66(3): 383−402. https://doi. org/10.1016/s0016-

7037(01)00791-8

Woodland, S. J., Rehkämper, M., Halliday, A. N., et al., 2005. Accurate Measurement of Silver Isotopic Compositions in Geological Materials Including Low Pd/Ag Meteorites. *Geochimica et Cosmochimica Acta*, 69(8): 2153−2163. https://doi.org/10.1016/j.gca.2004.10.012

Xie, G. Q., Mao, J. W., Li, R. L., et al., 2006. Geological Characteristics and Mineral Model of Skarn Fe Deposits from Southeastern Hubei Province, China. *Mineral Deposits*, 25(S1): 147−150. https://doi. org/10.16111/j.0258-7106.2006.s1.039 (in Chinese with English Abstract)

Xu, Z. F., Zeng, Z. H., 2006. Discussions on Relationship between Mineralization and Magmatism in Qixiashan Pb-Zn-Ag Ore Deposit of Nanjing. *Jiangsu Geology*, 30(3): 177−182 (in Chinese with English Abstract)

Yang, L., Dabek-Zlotorzynska, E., Celo, V., 2009. High Precision Determination of Silver Isotope Ratios in Commercial Products by MC-ICP-MS. *Journal of Analytical Atomic Spectrometry*, 24(11): 1564−1569. https://doi.org/10.1039/b911554d

Yang, L., Sturgeon, R. E., Mester, Z., et al., 2010. Metrological Triangle for Measurements of Isotope Amount Ratios of Silver, Indium, and Antimony Using Multicollector-Inductively Coupled Plasma Mass Spectrometry: The 21st Century Harvard Method. *Analytical Chemistry*, 82(21): 8978−8982. https://doi.org/10.1021/ac1019396

Zhang, G. S., 1998. Characteristics of the Structures and Their Rock and Ore Control Low. *Hubei Geology & Mineral Resources*, 12(2): 16−23. https://doi. org/10.16536/j. cnki. issn. 1671-1211.1998.02.004 (in Chinese with English Abstract)

Zhang, J. Z., 2013. Geology, Exploration Model and Practice of Zijinshan Ore Concentrated Area. *Mineral Deposits*, 32(4): 758−767. https://doi. org/10.16111/j. 0258-7106.2013.04.009 (in Chinese with English Abstract)

Zhang, T., Lu, D., Zeng, L., et al., 2017. Role of Secondary Particle Formation in the Persistence of Silver Nanoparticles in Humic Acid Containing Water under Light Irradiation. Environmental Science & Technology, 51(24): 14164−14172. https://doi. org/10.1021/acs. est.7b04115

Zhong, J., Chen, Y. J., Qi, J. P., et al., 2017. Geology, Fluid Inclusion and Stable Isotope Study of the Yueyang Ag-Au-Cu Deposit, Zijinshan Orefield, Fujian Province, China. *Ore Geology Reviews*, 86: 254−270. https://doi.org/10.1016/j.oregeorev.2017.02.023

Zhu, D. G., Lu, G. X., Deng, J., et al., 1999. Discussion on the Geology and Genesis of Dazhuangzi Gold Deposit in Eastern Shandong Province. *Journal of Precious Metallic Geology*, 8(2): 18−23. https://doi. org/10.13686/j.cnki.dzyzy.1999.02.004 (in Chinese with English Abstract)

Zhu, Y. F., Dong, G.,Liu, X.,et al., 2021. Progress of Silver Isotopes Studies in Planetary and Earth Sciences. *Earth Science*, 46(12): 4390-4404. https://doi.org/10.3799/dqkx.2021.080